

Physicochemical and electrochemical characterization of hybrid cellulose separators for aqueous zinc-ion batteries

Downloaded from: https://research.chalmers.se, 2026-11-02 13:23 UTC

Citation for the original published paper (version of record):
Afiandika, M., Zitting, A., Sonker, A. et al (2026). Physicochemical and electrochemical characterization of hybrid cellulose separators for aqueous zinc-ion batteries. Materials Chemistry Frontiers, 10(20): 3832-3840.
http://dx.doi.org/10.1039/d6qm00644b

N.B. When citing this work, cite the original published paper.

research.chalmers.se offers the possibility of retrieving research publications produced at Chalmers University of Technology. It covers all kind of research output: articles, dissertations, conference papers, reports etc. since 2004. research.chalmers.se is administrated and maintained by Chalmers Library

(article starts on next page)

MATERIALS CHEMISTRY
FRONTIERS

RESEARCH ARTICLE

Published on 08 September 2026
Licensed under CC-BY 4.0

Check for updates

Cite this: *Mater. Chem. Front.*, 2026, **10**, 3832

Physicochemical and electrochemical characterization of hybrid cellulose separators for aqueous zinc-ion batteries

Marita Afiandika,[ae] Aleksi Zitting,[ae] Amit Kumar Sonker,[b] Shizhao Xiong,[c] Gunnar Westman[de] and Aleksandar Matic*[ae]

In aqueous zinc ion batteries, the use of Zn metal as the anode has been hindered by the inhomogeneous deposition of Zn and the growth of Zn structures that can pierce the separator. Here, we present a functional separator based on cellulose nanocrystals (CNC) and TEMPO-oxidized cellulose nanofibrils (TCNF) to regulate the nature of Zn deposition and thereby battery performance. The incorporation of TCNF enhances the ductility, electrolyte uptake, and ionic conductivity, while small- and wide-angle X-ray scattering (SAXS/WAXS) analysis confirms swelling of the CNC : TCNF structure when soaking in an aqueous electrolyte, but also that the swelling is limited. With an optimized weight ratio between CNC and TCNF (5 : 1), a longer cycle life at high current density (10 mA cm^{-2}) and areal capacity (5 mAh cm^{-2}) is achieved, compared to when a commercial filter paper separator is used. This work highlights the potential of forest biomaterials in the functionalization of separators for enhancing the cycle life of aqueous zinc ion batteries.

Received 17th July 2026,
Accepted 7th September 2026

DOI: 10.1039/d6qm00644b

rsc.li/frontiers-materials

Introduction

The development of rechargeable batteries using zinc (Zn) metal anodes has been the focus of research for more than a decade since Xu *et al.* presented the concept of the Zn-ion battery (ZIB) in 2012.[1] However, the cycle life of aqueous ZIBs has been limited by uneven Zn deposition and stripping, and by growth of dendrites that can pierce the separator and cause battery failure during charge.[2–4] Numerous efforts have been reported to mitigate these issues, such as coating of the metal anode[5] and tuning the electrolyte formulation.[6] The former is often pursued to protect the zinc metal anode from corrosion and hydrogen evolution reaction, and has more recently developed into artificial layers with hybrid architectures.[7–9] Electrolyte formulation is commonly used either to tune the first solvation shell of Zn^{2+} and the electric double layer, or to lower the activity of free water, which drives parasitic side reactions such as hydrogen evolution and corrosion.[10,11] The separator, in contrast, is an existing cell component that lies directly in the ion transport path, and although often disregarded as a passive component, it can regulate Zn^{2+} flux and significantly influence the cycling stability of Zn-ion batteries.[12,13]

Glass fibre and filter paper are the two most common separators utilised for aqueous ZIBs.[14] However, both separators commonly have thicknesses on the order of hundred micrometres, which will decrease the volumetric energy density on cell level.[15] Although glass fibre has good wettability towards aqueous electrolytes,[16] it has an uneven pore distribution, leading to inhomogeneous metal deposition at the anode during charge.[17] Meanwhile, the mechanical strength of filter paper decreases considerably when soaked with the electrolyte and cannot withstand dendrite propagation.[18] To overcome these drawbacks, several strategies have been introduced to modify the properties of both glass fibre and filter paper separators, such as the incorporation of nanoparticles[19,20] or introducing an additional coating.[21,22] These examples highlight the necessity of separator functionalization, emphasizing its role beyond being a passive component in the battery.

Various polymers have been investigated to develop functional separators that enhance mechanical robustness and inhibit dendrite growth,[23] often by combining two components so that mechanical and interfacial requirements are met by different parts of the structure, as is common in composite polymer electrolyte design.[24] Among these polymers, cellulose-

[a] *Department of Physics and Astronomy, Chalmers University of Technology, Gothenburg 41296, Sweden. E-mail: matic@chalmers.se*
[b] *BA54 Biomaterials Processing and Products, VTT Technical Research Centre of Finland, Future Hub, Tekniikantie 21, Espoo 02150, Finland*
[c] *Faculty of Material Science and Engineering, Kunming University of Science and Technology, Kunming 650093, China*
[d] *Department of Chemistry and Chemical Engineering, Chalmers University of Technology, Gothenburg 41296, Sweden*
[e] *Wallenberg Wood Science Centre, Chalmers University of Technology, Gothenburg 41296, Sweden*

 This journal is © The Royal Society of Chemistry and the Chinese Chemical Society 2026

based materials have been widely explored due to the abundance of cellulose, combined with low-cost and excellent wettability for aqueous electrolytes due to the presence of hydroxyl groups that promote aqueous electrolyte uptake.[25] Cellulose nanocrystals (CNC)[26,27] and cellulose nanofibrils (CNF)[28,29] are often used as building blocks for battery separators. Materials made entirely of CNC are commonly more brittle than other cellulose-based materials, such as CNF-based membranes, due to their high crystallinity and relatively uniform rod-like structure, which limits entanglement and results in the formation of small pores.[30–32] This brittleness makes material handling challenging.[33,34] On the other hand, CNF produced by TEMPO-mediated oxidation (2,2,6,6,-tetramethylpipelidine-1oxyl radical) is less crystalline, compared to CNC, and can form an entangled fibre network enabling the formation of flexible films, but usually with lower mechanical strength.[35] Although cellulose-based materials have attracted increasing attention for ZIBs, there remains a need to develop new formulations that can enable thin, yet strong films that are compatible with Zn-metal anodes.

A particular advantage of cellulose-based materials for battery separators is the possibility to combine different types of building blocks, as well as utilising functionalisation, which allows tuning mechanical robustness and Zn deposition. In this work, we report a new concept with hybrid separators composed of CNC and TCNF, referred to as HCT separators, prepared by straightforward evaporation-induced self-assembly. The combined effects of CNC and TEMPO-oxidized cellulose nanofibrils (TCNF) to improve electrochemical performance, mechanical strength, and electrolyte uptake have not yet been systematically studied for separators. We vary the weight ratio of CNC : TCNF to optimize mechanical properties, electrolyte uptake, and ion conductivity. We also explore the structural properties using small- and wide-angle X-ray scattering (SAXS/WAXS) and evaluate the electrochemical performance.

Results and discussion

Fig. 1a shows a schematic of the preparation procedure of the HCT separators using evaporation-induced self-assembly. The preparation is straightforward, comprising physical mixing of a precursor aqueous solution, homogenization and casting to obtain a free-standing separator after solvent (water) evaporation at room temperature. The resulting transparent HCT separators are shown in Fig. S1a–c (SI). The typical thickness of the HCT separators is 30–45 μm (Table S1), corresponding to approximately 25% of the thickness of the Whatman grade 5 filter paper used as the reference separator (178 μm, experimentally measured (Fig. S2a)). The surface morphology of the HCT separators was characterized using scanning electron microscopy (SEM), and all separators exhibit reasonably smooth surfaces with no visible pores (Fig. 1b–d), confirming good film-forming properties.[36] With increasing TCNF content, the surface appears rougher. This can be attributed to the tendency of fibrils to agglomerate, which has been reported to result in uneven membrane surfaces at higher CNC : CNF weight ratios (*e.g.* 1 : 4).[37] In comparison, the filter paper has an uneven surface with large pores (Fig. S2b and c).

Fourier-transform infrared spectroscopy (FTIR) was used to investigate the chemical structure and intermolecular interactions in the HCT separators. Full spectra are shown in Fig. S3a. The spectra from all separators display characteristic bands of cellulose; the band assignments can be found in Table S2. Fig. 1e shows the spectral region of the water bending band (1645 cm^{-1}) from the water molecules commonly present in cellulose materials, and a band from carboxylate groups (−COONa) (1602 cm^{-1}) from TCNF.[38,39] The carboxylate band

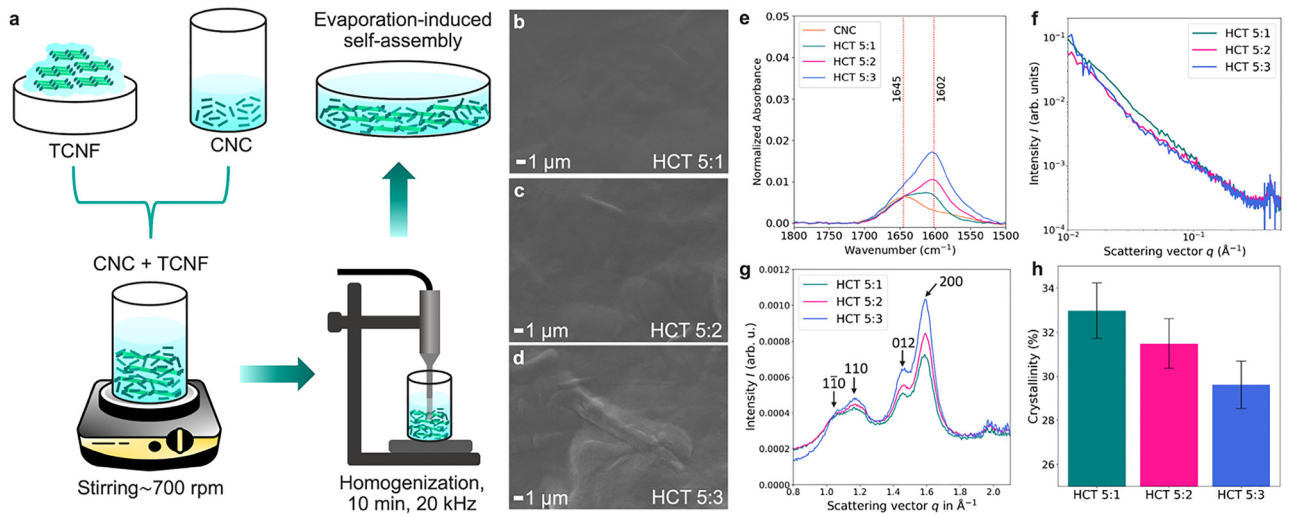


Fig. 1 (a) Schematic of preparation of HCT separators through evaporation-induced self-assembly. (b)–(d) SEM images of the surface morphology of HCT separators with CNC:TCNF weight ratios (b) 5 : 1, (c) 5 : 2 and (d) 5 : 3. (e) FTIR spectra of HCT and pure CNC separators in the range 1800–1500 cm^{-1}. Red dashed lines indicate the positions of water bending band at 1645 cm^{-1} and band from carboxylate groups. (f) SAXS and (g) WAXS profiles from HCT separators. (h) Estimated crystallinity of HCT separators, obtained by fitting WAXS spectra from dry separators measured under vacuum.

grows in intensity upon the addition of TCNF (Fig. 1e), showing the successful incorporation of TCNF in the hybrid separators.

Fig. 1f shows the SAXS profile from the HCT separators. The SAXS profiles from dry samples (before immersion in electrolyte) are almost featureless, with the scattering intensity following a power-law decay. A fit of $I(q) \propto q^{-\alpha}$ to the low q region gives an exponent $\alpha \approx 3$, which could come from rough surfaces or densely packed structures. As CNC are rigid polymer fragments and TCNF are flexible polymers, the likely explanation is that this scattering behaviour comes from densely packed structures, similar to collapsed polymer network. There is an increase in the signal at higher q leading to a small shoulder, which is more visible in the SAXS profile from a separator with only CNC present, where the feature is found at q =0.1 Å^{-1} (Fig. S3b). For the HCT separators, the shoulder is less pronounced, likely due to the presence of TCNF, which can fill previously unoccupied regions with its flexible chains, reducing scattering contrast. The WAXS profiles (Fig. 1g) show the major crystalline peaks of the cellulose I_β phase, with no indication of other crystalline phases of cellulose present.[40] The crystallinity of the HCT separators was estimated from the ratio of the integrated crystalline peak area to the total integrated WAXS area, including the amorphous contribution, following previously reported methods (Fig. S3c).[41] Since the amorphous background is sensitive to moisture content, the crystallinity was determine from WAXS experiments performed in vacuum. As expected, there is a decrease in the crystallinity with increasing TCNF content (Fig. 1h), since TCNF is more amorphous compared to CNC (Fig. S3d).[42]

Fig. 2a shows the stress–strain curves from mechanical tests on the HCT separators, and the values of tensile strength and strain at break are reported in Table S3. The addition of TCNF to CNC increases the tensile strength at break. With increasing TCNF content, the tensile strength decreases, but the strain at break increases, which reflects the decreased brittleness with the addition of TCNF. It is also worth noting that the HCT

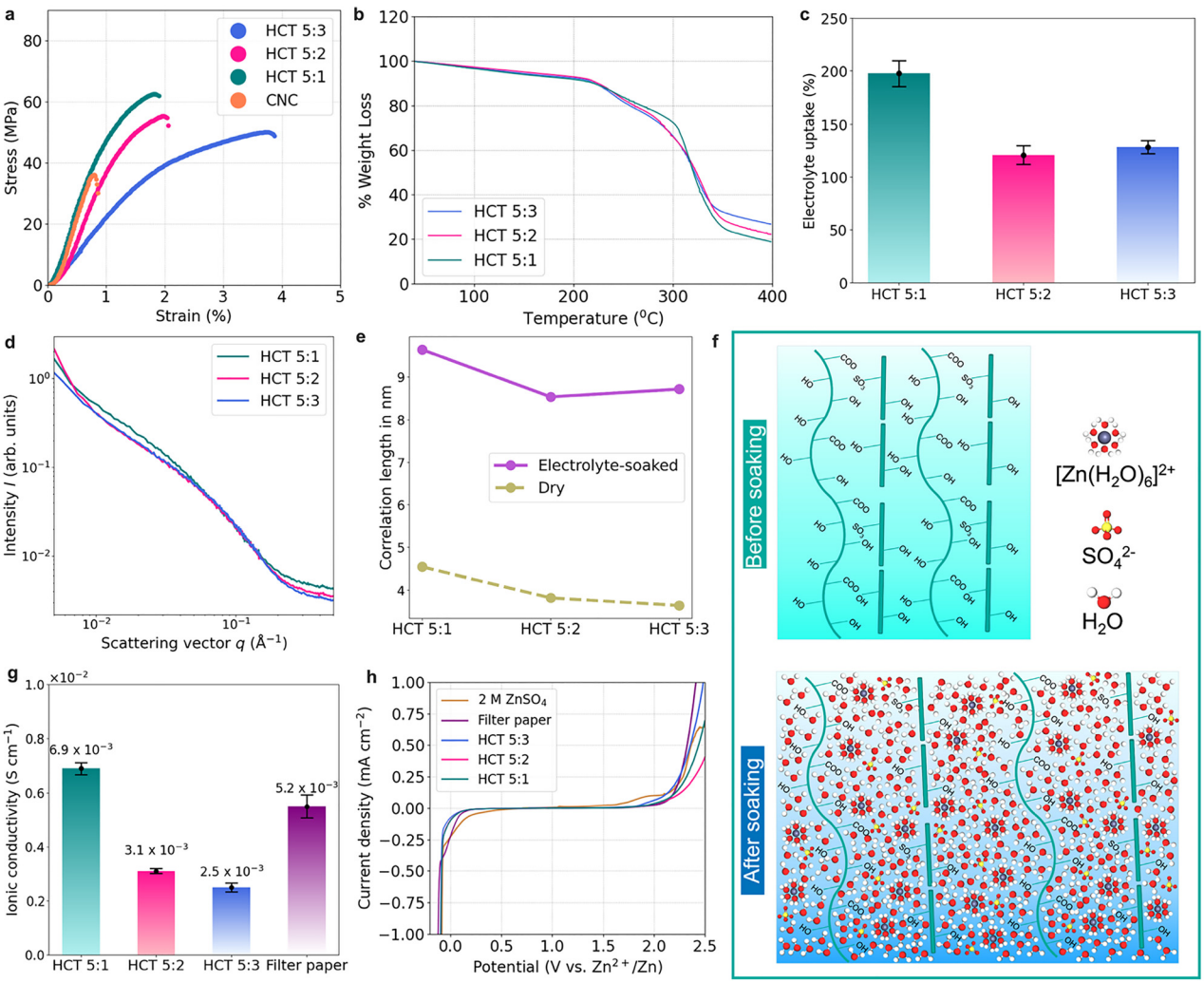


Fig. 2 (a) Stress–strain curves, (b) TGA curves, and (c) electrolyte uptake of HCT separators. (d) SAXS curves from HCT separators soaked in electrolyte. (e) Estimated correlation length based on Kratky analysis. (f) Schematic illustration of the structure of separators before and after soaking in electrolyte. (g) Ionic conductivity at room temperature and (h) LSV curves of Zn||Ti cells using bare 2 M $ZnSO_4$ aqueous electrolyte, and various HCT and filter paper separators soaked in the same electrolyte.

 This journal is © The Royal Society of Chemistry and the Chinese Chemical Society 2026

separators exhibit enhanced mechanical flexibility (Fig. S4a), as evidenced by a higher strain at break compared to separator made up of only CNC (Fig. 2a) and commercial Whatman grade 5 filter paper (Fig. S4b). This improvement is beneficial with respect to mitigating growth of Zn dendrites through the separator.[43] Furthermore, in the swollen state HCT 5 : 1 retains a tensile strength of 9.6 MPa, compared to ~2 MPa for filter paper under the same conditions (Fig. S4b), indicating that the mechanical integrity of the separator is maintained when soaked in the electrolyte.

To compare the thermal stability of the HCT separators, thermogravimetric analysis (TGA) was performed under N_2 flow (Fig. 2b). Overall, the results show that the HCT separators are thermally stable at temperatures relevant for ZIBs (<80 °C).[44,45] Initially, up to 200 °C, a small, almost linear weight loss is observed that can be attributed to water that is always present in cellulose-based materials.[46] At approximately 220 °C, a step in the TGA curve is observed, which is most likely related to the degradation of carboxyl groups of TCNF.[38,39,47] At higher temperatures, a second step around 320 °C is related to pyrolysis or depolymerization of the cellulose backbone.[48,49]

Fig. 2c compares the electrolyte uptake of the HCT separators. HCT 5 : 1 shows the highest electrolyte uptake (almost 200% of weight), but with increasing the TCNF content, the uptake decreases. The electrolyte uptake is comparable with what has previously been reported for cellulose-based separators for aqueous ZIBs.[50] Although porosity generally impacts electrolyte uptake, the estimated porosity values of the HCT separators are quite similar, 36% for HCT 5 : 1 and HCT 5 : 2 and 33% for HCT 5 : 3 (Fig. S4c). This suggests that electrolyte uptake is not only influenced by porosity but that swelling of the polymer matrix also occurs.

Fig. 2d shows the SAXS curves of the HCT separators soaked in the electrolyte. A clear shoulder can be observed in the SAXS curves induced by the swelling of the structure, indicating changes in the spatial arrangement of cellulose crystals and/or fibrils. Kratky analysis (Fig. S5a and b) was used to estimate the correlation length related to the shoulder, and the results are shown in Fig. 2e. In the dry state, the correlation length falls between 3.5 and 4.5 nm and decreases modestly with increasing TCNF content. The presence of a measurable correlation length, corresponding to the characteristic spacing between fibrils, provides further support for the $\alpha \approx 3$ exponent in Fig. 1f, reflecting a densely packed structure with broadly distributed spacing rather than interfacial roughness. After electrolyte soaking, the correlation length rises to 8.5–9.6 nm, a roughly twofold increases over the dry state. Thus, electrolyte uptake causes a considerable swelling of the structure of the membranes. To better understand the effect of swelling, Fig. S5c shows SAXS profiles from HCT separators soaked in water. The shoulder is more pronounced for the water-soaked separators and is also found at lower q, reflecting a larger correlation length, around 17 nm. This is roughly twice that of the electrolyte-soaked separators and four times the dry state. This more extensive swelling is accompanied by a softening of the separator, although it remains free-standing. The reduced swelling in the electrolyte compared to the swelling in water can be attributed to interactions between the electrolyte ions and the charged cellulose network. Zn^{2+} ions can coordinate to the carboxylate groups of TCNF,[51,52] forming ionic crosslinks between fibrils that reduce their electrostatic repulsion and restrict network expansion. Fig. 2f illustrate the effect of soaking in 2 M $ZnSO_4$ aqueous electrolyte on the structure of the HCT separators.

The ionic conductivity follows a similar trend (Fig. 2g) with the electrolyte-soaked HCT 5 : 1 separator showing the highest ionic conductivity (6.9×10^{-3} S cm^{-1}), reflecting its high electrolyte uptake. In comparison, the HCT 5 : 2 and HCT 5 : 3 separators show considerably lower ionic conductivity, which can not only be explained by a lower electrolyte uptake. An increased fibril entanglement with the increased TCNF content could also induce more tortuous conduction pathways, as well as too strong coordination between Zn^{2+} and carboxyl groups in TCNF.

Fig. 2h shows the results from linear sweep voltammetry experiments, used to evaluate the electrochemical stability window for the separators soaked in a 2 M $ZnSO_4$ aqueous electrolyte. A filter paper separator and the bare electrolyte were included as references. Using a cutoff of 0.2 mA cm^{-2}, all HCT separators exhibit anodic onsets comparable to filter paper, indicating that oxidative stability is not compromised relative to this reference. The resulting windows are fully compatible with the voltage range of most ZIBs. For instance, the typical operating voltage is 0.4–1.4 V for a V_2O_5 cathode[53] and 0.8–1.8 V for a MnO_2 cathode.[54] A weak anodic feature at ~1.8–2.1 V present in the bare electrolyte is absent in all separator-containing cells, suggesting that the presence of a cellulose based separator reduces the availability of free water at the electrode–electrolyte interface, supressing water electrolysis. A similar result has been reported for a cellulose nanofibril separators with $ZnSO_4$ electrolyte.[55] Since both HCT and filter paper separators are cellulose-based, this suppression is therefore not specific to the HCT composition.

Based on the higher electrolyte uptake, ionic conductivity, and mechanical strength, the HCT 5 : 1 separator was selected for further electrochemical characterization. To investigate Zn plating and stripping, symmetric Zn||Zn cells were assembled using the HCT 5 : 1 separator soaked in 2 M $ZnSO_4$ aqueous electrolyte. Cells with Whatman grade 5 filter paper are included for comparison. Fig. 3a shows the cycling stability, where the Zn||Zn cell with the HCT 5 : 1 separator showed stable cycling at current densities up to 10 mA cm^{-2}, at an areal capacity of 5 mAh cm^{-2}. In contrast, the Zn||Zn cell with the filter paper separator short-circuited already after 75 h at the lowest current density (1 mA cm^{-2}). The excellent performance of the cell with the HCT 5 : 1 separator is further underlined by long-term cycling at a high current density and areal capacity (10 mA cm^{-2} and 5 mAh cm^{-2}) (Fig. 3b), sustaining the high current and high capacity for more than 330 h compared to only 9 h for the cell with the filter paper separator. Even at lower current density (0.5 mA cm^{-2}) and low areal capacity (1 mAh cm^{-2}), the cell with the filter paper separator short-circuited early (Fig. S6a).

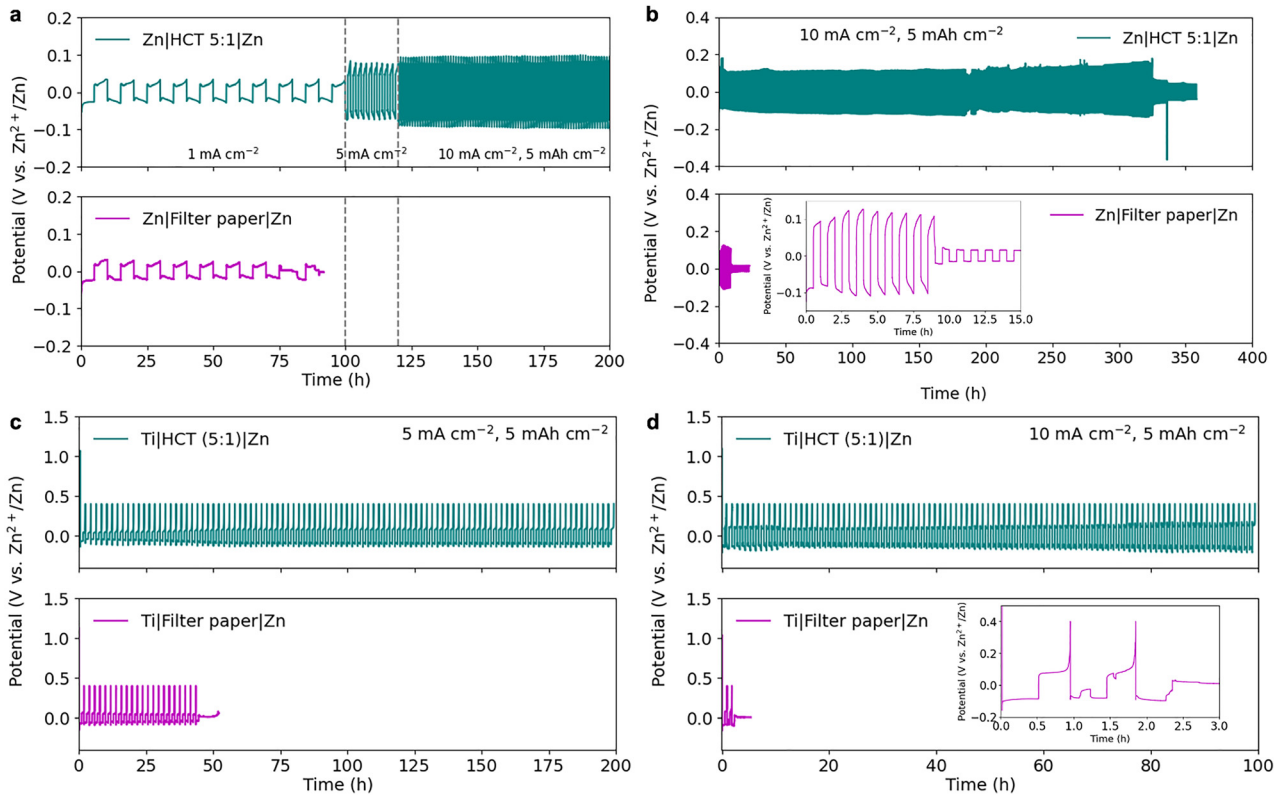


Fig. 3 (a) Rate performance of Zn||Zn cells with HCT 5 : 1 and filter paper separators at current densities of 1, 5, and 10 mA cm^{-2} at areal capacity of 5 mAh cm^{-2}. (b) Long term cycling performance of Zn||Zn cells with HCT 5 : 1 and filter paper separators at 10 mA cm^{-2} and 5 mAh cm^{-2}. (c) and (d) Zn||Ti cells with HCT 5 : 1 and filter paper at a fixed areal capacity of 5 mAh cm^{-2} and two current densities (c) 5 mA cm^{-2} and (d) 10 mA cm^{-2}.

The reversibility of Zn deposition/stripping in terms of the coulombic efficiency (CE) was evaluated by galvanostatic cycling of Zn||Ti cells. Fig. 3c and d show the voltage response at 5 and 10 mA cm^{-2}, at a fixed areal capacity of 5 mAh cm^{-2}. The cell with the HCT 5 : 1 separator showed an average CE of 99% at both current densities over 100 cycles (Fig. S6b and c). In contrast, the Zn||Ti cell with the filter paper separator short-circuited early. These results demonstrate that the HCT 5 : 1 separator can mitigate problems with uneven Zn deposition and corrosion/passivation, which limit the cycle life and lower the CE in cells with aqueous electrolytes.[56–58]

The role of the HCT 5 : 1 separator in regulating Zn deposition was further investigated by SEM imaging of the morphology of electrodeposited Zn on Ti substrates (1 mAh cm^{-2} at a current density of 10 mA cm^{-2}, Fig. 4a–j). SEM images of pristine Ti (Fig. 4a and d) and Zn deposited on Ti in cells with HCT 5 : 1 (Fig. 4b and e) and filter paper (Fig. 4c and f) separators reveal clear differences. The electrode cycled with the HCT 5 : 1 separator shows uniform deposition, whereas the filter paper results in highly nonuniform growth. Since the Ti substrate, electrolyte, and deposition conditions were identical in both cases, this difference must originate from how Zn^{2+} is transported through the separator rather than from any change in the intrinsic deposition behaviour of the substrate. This is consistent with reports that deposit morphology is governed primarily by the spatial distribution of Zn^{2+} at the electrode surface,[59] and that oxygen-containing surface groups can promote a more regular distribution of Zn^{2+} and thereby more uniform deposition.[60] In the HCT separator, the carboxylate groups introduced by TCNF provide the most plausible site of interaction, given that carboxylate can preferentially coordinate Zn^{2+} over water at the electrode/electrolyte interface.[61] In the HCT separator these groups are immobilised on the fibril network, so the interaction occurs as Zn^{2+} passes through the separator rather than in bulk solution. Images of the separators extracted from the cycled cells further highlight this result (Fig. 4g–i). Due to the nonuniform and big pore size of filter paper, trapped deposits are found inside the pores (Fig. 4g), while the HCT 5 : 1 separator shows minor surface features with no deposits penetrating into the separator (Fig. 4h and i).

To assess the practical applicability of the HCT 5 : 1 separator, full cells with KVO ($K_{0.5}V_2O_5$) cathodes (loading 5.4–6.1 mg cm^{-2}) were assembled. The Zn||KVO cell with the HCT 5 : 1 separator showed a discharge capacity around 150 mAh g^{-1} at a current density of 0.5 A g^{-1} (corresponding to 3.0 mA cm^{-2}), Fig. 4j. The cycling performance (Fig. 4k) shows an initial capacity decay during the first 10 cycles, followed by recovery and stabilization around 150 mAh g^{-1} over 100 cycles. At a higher current density (1 A g^{-1}, 5.4 mA cm^{-2}), Fig. S7a and b, the cell had a discharge capacity of 110 mAh g^{-1} over 100 cycles. For comparison, Zn||KVO cells assembled with a filter paper separator showed lower capacity at both 0.5 and 1 A g^{-1} (Fig. S8a–d). At 0.5 A g^{-1}, the

 This journal is © The Royal Society of Chemistry and the Chinese Chemical Society 2026

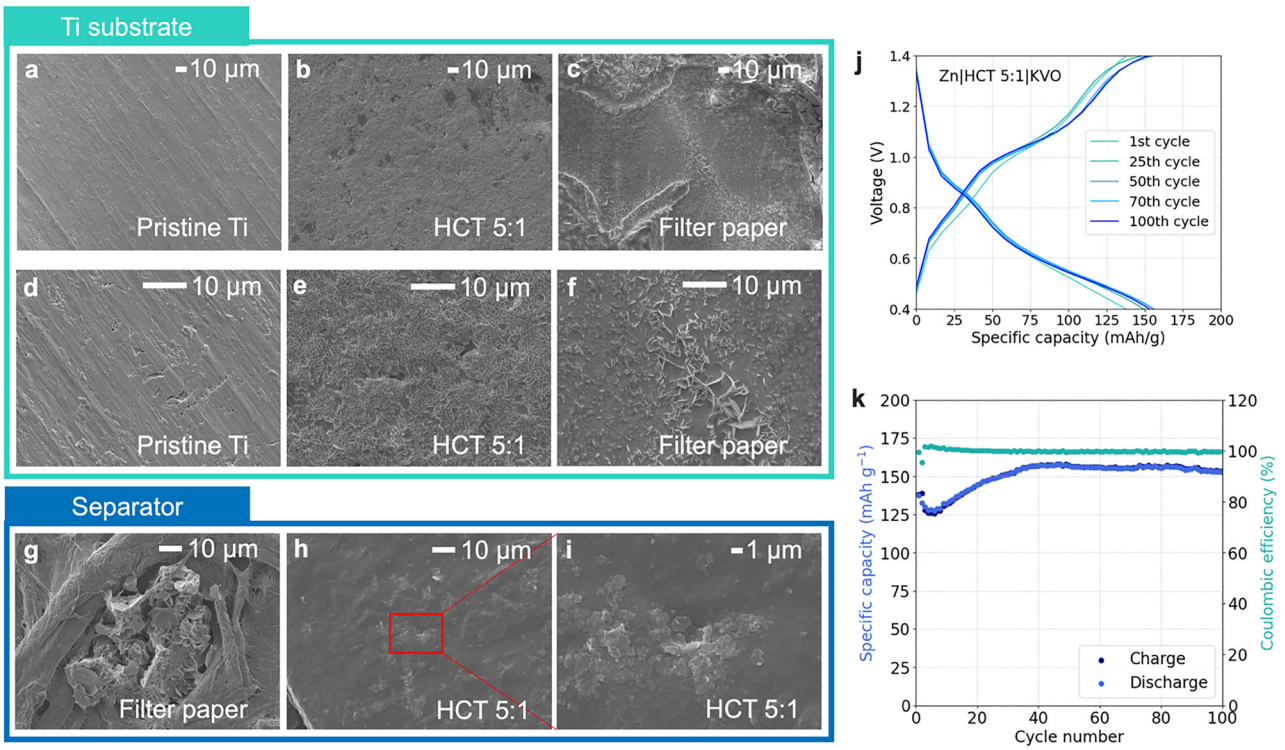


Fig. 4 SEM images of Ti substrates (a) pristine and after Zn deposition in presence of (b) HCT 5 : 1 separator and (c) filter paper separator at 10 mA cm^{-2} and 1 mAh cm^{-2}. (d)–(f) Higher magnifications of (a)–(c). Surface morphology of cycled separators: (g) filter paper and (h) HCT 5 : 1 separator, and (i) higher magnification of (h). (j) Galvanostatic discharge and charge profiles and (k) cycling performance of Zn||KVO with HCT 5 : 1 separator at a current density of 0.5 A g^{-1}.

cell exhibits erratic coulombic efficiency, indicating soft short circuiting (Fig. S8a and b). At 1 A g^{-1}, an isolated event of the same type occurs after 80 cycles (Fig. S8c and d). The initial capacity decay followed by recovery is also observed in the filter paper cells (Fig. S8b and d), indicating that it originates from the KVO cathode rather than the separator. The decay is consistent with the structural rearrangement and partial dissolution commonly reported for vanadium-based cathodes in mild aqueous Zn^{2+} electrolytes,[62–64] while the subsequent recovery is attributed to gradual electrochemical activation of the cathode, which is well documented for vanadium oxide and is expected to be more pronounced for the relatively thick electrodes used here.[65,66] The discharge capacities are slightly lower compared to literature,[67] likely due to higher cathode loading used in this work, 5–6 mg cm^{-2}, compared to 3 mg cm^{-2} in ref. 67 which increases electrode thickness and can introduce mass-transport and kinetic limitations.[68] The results nonetheless show the potential of the HCT (5 : 1) separator for practical application in aqueous Zn-ion batteries.

Conclusions

Hybrid separators composed of CNC and TCNF were successfully prepared *via* evaporation-induced self-assembly at different CNC : TCNF ratios. The addition of TCNF significantly enhanced the ductility, electrolyte uptake and ionic conductivity. SAXS/WAXS analysis showed limited swelling of the CNC : TCNF structure when soaking in the aqueous electrolyte, considerably less than in water. Electrochemical tests demonstrated that Zn||Zn and Zn||Ti cells using a hybrid separator with a 5 : 1 CNC : TCNF weight ratio could sustain long-term cycling at practical conditions (5 mAh cm^{-2}, 10 mA cm^{-2}) with a coulombic efficiency of 99%. Furthermore, a Zn||KVO full cell with the HCT 5 : 1 separator exhibited stable performance for more than 100 cycles, with discharge capacities of 150 and 110 mAh g^{-1} at 0.5 and 1 A g^{-1}, respectively, at the 100th cycle.

Author contributions

M. A.: conceptualization, methodology, investigation, formal analysis, validation, visualization, writing – original draft, writing – review & editing. A. Z.: investigation, formal analysis, writing – original draft (SAXS-WAXS data analysis and discussion), writing – review & editing. A. K.: conceptualization, methodology, resources (TCNF preparation), writing – review & editing. S. X.: conceptualization, methodology, writing – review & editing. G. W.: conceptualization, methodology, resources (CNC preparation), writing – review & editing. A. M.: conceptualization, supervision, project administration, funding acquisition, resources, writing – review & editing.

Conflicts of interest

There are no conflicts to declare.

Data availability

All data can be found in the main article or the SI. Supplementary information (SI) is available. See DOI: https://doi.org/10.1039/d6qm00644b.

Acknowledgements

The authors acknowledge funding from the Knut and Alice Wallenberg Foundation (KAW) through the Wallenberg Wood Science Center. This work was performed in part at the Chalmers Material Analysis Laboratory, CMAL.

References

1 C. Xu, B. Li, H. Du and F. Kang, Energetic Zinc Ion Chemistry: The Rechargeable Zinc Ion Battery, *Angew. Chem., Int. Ed.*, 2012, **51**, 933–935.
2 Q. Li, Y. Zhao, F. Mo, D. Wang, Q. Yang, Z. Huang, G. Liang, A. Chen and C. Zhi, Dendrites issues and advances in Zn anode for aqueous rechargeable Zn-based batteries, *EcoMat*, 2020, **2**, e12035.
3 Z. Hong, Z. Ahmad and V. Viswanathan, Design Principles for Dendrite Suppression with Porous Polymer/Aqueous Solution Hybrid Electrolyte for Zn Metal Anodes, *ACS Energy Lett.*, 2020, **5**, 2466–2474.
4 J. Yang, B. Yin, Y. Sun, H. Pan, W. Sun, B. Jia, S. Zhang and T. Ma, Zinc Anode for Mild Aqueous Zinc-Ion Batteries: Challenges, Strategies, and Perspectives, *Nano-Micro Lett.*, 2022, **14**, 42.
5 H. Yoon, C. Choi, S. Hong, M. Afiandika, A. Matic, T. G. Yun and B. Hwang, Acid-Treatment-Assisted Liquid Metal–Based Zinc Metal Anode for Stable Aqueous Zinc-Ion Batteries, *Int. J. Energy Res.*, 2025, **2025**, 1405163.
6 M. Palluzzi, M. Afiandika, S. Xiong, A. Tsurumaki, P. D'Angelo, A. Matic and M. A. Navarra, A low-transition-temperature electrolyte based on ethylene glycol for rechargeable zinc-ion batteries, *Electrochim. Acta*, 2025, **525**, 146061.
7 Z. Chen, B. Xiang, P. Wang, Z. Yang, C. Tsui, C. Tang, M. Wang, Y. Zhu and Y. Yang, Modular Interfacial Engineering via Nanofiber-Reinforced Hydrogels for Stabilizing Zn Anodes Toward High-Performance Zn-Based Batteries, *Energy Environ. Mater.*, 2026, e70391.
8 Y. An, B. Xu, Y. Tian, H. Shen, Q. Man, X. Liu, Y. Yang and M. Li, Reversible Zn electrodeposition enabled by interfacial chemistry manipulation for high-energy anode-free Zn batteries, *Mater. Today*, 2023, **70**, 93–103.
9 Y. Tian, Y. An, Y. Yang and B. Xu, Robust nitrogen/selenium engineered MXene/ZnSe hierarchical multifunctional interfaces for dendrite-free zinc-metal batteries, *Energy Storage Mater.*, 2022, **49**, 122–134.
10 J. Cao, D. Zhang, X. Zhang, Z. Zeng, J. Qin and Y. Huang, Strategies of regulating Zn^{2+} solvation structures for dendrite-free and side reaction-suppressed zinc-ion batteries, *Energy Environ. Sci.*, 2022, **15**, 499–528.
11 J. Geng, X. Liu, R. Tao, G. Huang, Y. Yang, H. Li, D. Wang, Z. Liu and J. Liang, Hydrophobic low-polarity perfluorobutanesulfonate shielding enhances the performance of aqueous Zn-ion batteries, *Mater. Chem. Front.*, 2026, **10**, 1947–1955.
12 B. Li, Y. Zeng, W. Zhang, B. Lu, Q. Yang, J. Zhou and Z. He, Separator designs for aqueous zinc-ion batteries, *Sci. Bull.*, 2024, **69**, 688–703.
13 B. Niu, D. Luo, X. He and X. Wang, Design and Conformation of Separators for High-performance Aqueous Zinc-Ion Batteries, *Chem. – Eur. J.*, 2024, **30**, e202402689.
14 Q. Nian, X. Yang, H. Hong, P. Chen, Y. Zhao, H. Lv and C. Zhi, Advancements in separator materials for aqueous zinc batteries, *Nanoscale Horiz.*, 2025, **10**, 1932–1955.
15 J.-Q. Huang, W. G. Chong and B. Zhang, Tackling the challenges of aqueous Zn-ion batteries via functional separator design, *J. Power Sources*, 2024, **594**, 234036.
16 L. Yang, M. Zhou, Y. Xie, X. Shen, S. Liang and G. Fang, Separators in aqueous zinc-ion batteries: Interfacial chemistry and optimization strategies, *Energy Storage Mater.*, 2024, **67**, 103271.
17 Y. Zhang, S. Yang, Y.-J. Zhu, D. Li, L. Cheng, H. Li and Z. Wang, Synergistically regulating the separator pore structure and surface property toward dendrite-free and high-performance aqueous zinc-ion batteries, *J. Colloid Interface Sci.*, 2024, **656**, 566–576.
18 L. Li, M. Sun, B. Hao, W. Chen, C. Zhu, L. Zhang, X. Shen, X. Zhou, J. Zhou, C. Yan, X. Liu and T. Qian, Dilemma of Low-Cost Filter Paper as Separator: Toughen Its Wet Strength for Robust Aqueous Zinc-Ion Batteries, *J. Phys. Chem. Lett.*, 2024, **15**, 380–390.
19 L. Li, J. Peng, X. Jia, X. Zhu, B. Meng, K. Yang, D. Chu, N. Yang and J. Yu, PBC@cellulose-filter paper separator design with efficient ion transport properties toward stabilized zinc-ion battery, *Electrochim. Acta*, 2022, **430**, 141129.
20 G. Lin, X. Zhou, L. Liu, H. Li, D. Huang, J. Liu, J. Li and Z. Wei, Performance improvement of aqueous zinc batteries by zinc oxide and Ketjen black co-modified glass fiber separators, *RSC Adv.*, 2023, **13**, 6453–6458.
21 X. Yang, W. Wu, Y. Liu, Z. Lin and X. Sun, Chitosan modified filter paper separators with specific ion adsorption to inhibit side reactions and induce uniform Zn deposition for aqueous Zn batteries, *Chem. Eng. J.*, 2022, **450**, 137902.
22 S. Liu, Q. Han, C. He, Z. Xu, P. Huang, L. Cai, H. Chen, H. Zheng, Y. Zhou, M. Wang, H. Tian, W.-Q. Han and H. Ying, Ion-Sieving Separator Functionalized by Natural Mineral Coating toward Ultrastable Zn Metal Anodes, *ACS Nano*, 2024, **18**, 25880–25892.
23 B.-S. Lee, S. Cui, X. Xing, H. Liu, X. Yue, V. Petrova, H.-D. Lim, R. Chen and P. Liu, Dendrite Suppression Membranes for Rechargeable Zinc Batteries, *ACS Appl. Mater. Interfaces*, 2018, **10**, 38928–38935.
24 J.-C. Wang, X.-Y. Liu, N. Zhang, P.-F. Wang, Y.-R. Zhu, J. Shu, C.-S. Li and T.-F. Yi, Constructing poly(ethylene oxide)-based composite solid electrolytes: starting from

 This journal is © The Royal Society of Chemistry and the Chinese Chemical Society 2026

the internal mechanism in batteries, *Mater. Chem. Front.*, 2024, **8**, 3446–3463.
25 L. Li, S. Jia, Z. Cheng and C. Zhang, Improved Strategies for Separators in Zinc-Ion Batteries, *ChemSusChem*, 2023, **16**, e202202330.
26 R. Gonçalves, E. Lizundia, M. M. Silva, C. M. Costa and S. Lanceros-Méndez, Mesoporous Cellulose Nanocrystal Membranes as Battery Separators for Environmentally Safer Lithium-Ion Batteries, *ACS Appl. Energy Mater.*, 2019, **2**, 3749–3761.
27 K. Kim, P. J. Kim, R. A. Chowdhury, R. Kantharaj, A. Candadai, A. Marconnet, V. G. Pol and J. P. Youngblood, Structural orientation effect of cellulose nanocrystals (CNC) films on electrochemical kinetics and stability in lithium-ion batteries, *Chem. Eng. J.*, 2021, **417**, 128128.
28 X. Ge, W. Zhang, F. Song, B. Xie, J. Li, J. Wang, X. Wang, J. Zhao and G. Cui, Single-Ion-Functionalized Nanocellulose Membranes Enable Lean-Electrolyte and Deeply Cycled Aqueous Zinc-Metal Batteries, *Adv. Funct. Mater.*, 2022, **32**, 2200429.
29 F. Brito Dos Santos, A. Whitbeck, A. Jalaee, J. Chalitangkoon, O. J. Rojas, E. Gyenge and E. J. Foster, Development of a robust ion-selective membrane from sulfonated cellulose nanofibers for zinc–iodine redox flow batteries, *J. Membr. Sci.*, 2025, **735**, 124486.
30 P. Molaiyan, S. Bhattacharyya, G. S. Dos Reis, R. Sliz, A. Paolella and U. Lassi, Towards greener batteries: sustainable components and materials for next-generation batteries, *Green Chem.*, 2024, **26**, 7508–7531.
31 B. Frka-Petesic, T. G. Parton, C. Honorato-Rios, A. Narkevicius, K. Ballu, Q. Shen, Z. Lu, Y. Ogawa, J. S. Haataja, B. E. Droguet, R. M. Parker and S. Vignolini, Structural Color from Cellulose Nanocrystals or Chitin Nanocrystals: Self-Assembly, Optics, and Applications, *Chem. Rev.*, 2023, **123**, 12595–12756.
32 Q. Chen, P. Liu, F. Nan, L. Zhou and J. Zhang, Tuning the Iridescence of Chiral Nematic Cellulose Nanocrystal Films with a Vacuum-Assisted Self-Assembly Technique, *Biomacromolecules*, 2014, **15**, 4343–4350.
33 J. Fernández-Santos, C. Valls, O. Cusola and M. B. Roncero, Improving Filmogenic and Barrier Properties of Nanocellulose Films by Addition of Biodegradable Plasticizers, *ACS Sustainable Chem. Eng.*, 2021, **9**, 9647–9660.
34 B. Natarajan, A. Krishnamurthy, X. Qin, C. D. Emiroglu, A. Förster, E. J. Foster, C. Weder, D. M. Fox, S. Keten, J. Obrzut and J. W. Gilman, Binary Cellulose Nanocrystal Blends for Bioinspired Damage Tolerant Photonic Films, *Adv. Funct. Mater.*, 2018, **28**, 1800032.
35 A. Isogai, T. Saito and H. Fukuzumi, TEMPO-oxidized cellulose nanofibers, *Nanoscale*, 2011, **3**, 71–85.
36 H. Wu, X. Wang, S. Li, Q. Zhang, M. Chen, X. Yuan, M. Zhou, Z. Zhang and A. Chen, Incorporation of cellulose nanocrystals to improve the physicochemical and bioactive properties of pectin-konjac glucomannan composite films containing clove essential oil, *Int. J. Biol. Macromol.*, 2024, **260**, 129469.
37 Y. Hua, T. Chen and Y. Tang, Preparation and characterization of nanocomposite films based on different ratios of cellulose nanocrystal and cellulose nanofiber, *Ind. Crops Prod.*, 2022, **179**, 114686.
38 K. Lichtenstein and N. Lavoine, Toward a deeper understanding of the thermal degradation mechanism of nanocellulose, *Polym. Degrad. Stab.*, 2017, **146**, 53–60.
39 E. Barnes, J. A. Jefcoat, E. M. Alberts, M. A. McKechnie, H. R. Peel, J. P. Buchanan, C. A. Weiss Jr., K. L. Klaus, L. C. Mimun and C. M. Warner, Effect of Cellulose Nanofibrils and TEMPO-mediated Oxidized Cellulose Nanofibrils on the Physical and Mechanical Properties of Poly(vinylidene fluoride)/Cellulose Nanofibril Composites, *Polymers*, 2019, **11**, 1091.
40 Y. Nishiyama, P. Langan and H. Chanzy, Crystal Structure and Hydrogen-Bonding System in Cellulose Iβ from Synchrotron X-ray and Neutron Fiber Diffraction, *J. Am. Chem. Soc.*, 2002, **124**, 9074–9082.
41 S. Park, J. O. Baker, M. E. Himmel, P. A. Parilla and D. K. Johnson, Cellulose crystallinity index: measurement techniques and their impact on interpreting cellulase performance, *Biotechnol. Biofuels*, 2010, **3**, 10.
42 X. Wang, C. H. Chang, J. Jiang, Q. Liu, Y. Liao, J. Lu, L. Li, X. Liu, J. Kim, A. Ahmed, A. E. Nel and T. Xia, The Crystallinity and Aspect Ratio of Cellulose Nanomaterials Determine Their Pro-Inflammatory and Immune Adjuvant Effects In Vitro and In Vivo, *Small*, 2019, **15**, 1901642.
43 Y. Huang, B. Wang, P. Xie, X. Qiu, J. Li, C. Xin, J. Liu and D. Chen, Bacterial cellulose mixed with glass fiber as a separator to achieve long cycle life of aqueous zinc-ion batteries, *J. Energy Storage*, 2025, **129**, 117395.
44 X. Li, H. Wang, X. Sun, J. Li and Y.-N. Liu, Flexible Wide-Temperature Zinc-Ion Battery Enabled by an Ethylene Glycol-Based Organohydrogel Electrolyte, *ACS Appl. Energy Mater.*, 2021, **4**, 12718–12727.
45 M. Chen, J. Chen, W. Zhou, X. Han, Y. Yao and C. Wong, Realizing an All-Round Hydrogel Electrolyte toward Environmentally Adaptive Dendrite-Free Aqueous Zn–MnO_2 Batteries, *Adv. Mater.*, 2021, **33**, 2007559.
46 K. S. Salem, V. Naithani, H. Jameel, L. Lucia and L. Pal, A systematic examination of the dynamics of water-cellulose interactions on capillary force-induced fiber collapse, *Carbohydr. Polym.*, 2022, **295**, 119856.
47 Z. Tang, X. Lin, M. Yu, A. K. Mondal and H. Wu, Recent advances in TEMPO-oxidized cellulose nanofibers: Oxidation mechanism, characterization, properties and applications, *Int. J. Biol. Macromol.*, 2024, **259**, 129081.
48 D. Trache, A. Donnot, K. Khimeche, R. Benelmir and N. Brosse, Physico-chemical properties and thermal stability of microcrystalline cellulose isolated from Alfa fibres, *Carbohydr. Polym.*, 2014, **104**, 223–230.
49 M. Li, B. He, Y. Chen and L. Zhao, Physicochemical Properties of Nanocellulose Isolated from Cotton Stalk Waste, *ACS Omega*, 2021, **6**, 25162–25169.
50 K. Zhang, S. Xie, J. Liang, Z. Zheng, Y. Li and L. Dong, Functional ultrathin separators enabling stable zinc anodes for lean-electrolyte zinc-ion batteries, *J. Membr. Sci.*, 2025, **722**, 123876.
51 H. Dong, J. F. Snyder, K. S. Williams and J. W. Andzelm, Cation-Induced Hydrogels of Cellulose Nanofibrils

with Tunable Moduli, *Biomacromolecules*, 2013, **14**, 3338–3345.
52 Y. Chen, P. Xie, B. Shen, H. Peng, L. Zhu, I. Shakir, G. Ma and Y. Xu, Hydrogel polymer electrolytes for advanced zinc-ion batteries: structural design and anode stabilization strategies, *Mater. Chem. Front.*, 2026, **10**, 2681–2725.
53 J. Zhou, L. Shan, Z. Wu, X. Guo, G. Fang and S. Liang, Investigation of V_2O_5 as a low-cost rechargeable aqueous zinc ion battery cathode, *Chem. Commun.*, 2018, **54**, 4457–4460.
54 T. Li, N. Zhang, B. Liu, P. Wang, Z. Liu, Y. Wang, D. Xu, H. Tian, Q. Zhang and T. Yi, Unlocking the Critical Role of Cations Doping in MnO_2 Cathode with Enhanced Reaction Kinetics for Aqueous Zinc Ion Batteries, *Adv. Funct. Mater.*, 2025, **35**, 2423755.
55 X. Shi, Y. Tan, Y. Zhang, Z. Long, C. Wang, L. Dai and C. Dong, Regulating Zn deposition via an ion-sieving, nanoporous cellulose separator for high performance aqueous zinc-ion batteries, *Int. J. Biol. Macromol.*, 2025, **287**, 138542.
56 C. Li, S. Jin, L. A. Archer and L. F. Nazar, Toward practical aqueous zinc-ion batteries for electrochemical energy storage, *Joule*, 2022, **6**, 1733–1738.
57 L. Ma, M. A. Schroeder, O. Borodin, T. P. Pollard, M. S. Ding, C. Wang and K. Xu, Realizing high zinc reversibility in rechargeable batteries, *Nat. Energy*, 2020, **5**, 743–749.
58 T. Sun, J. Yang, F. Kang, W. Zhang, J. Hui, X. Li and Q. Zhang, CNT-based electrodes for flexible aqueous zinc-ion batteries: progress and opportunities, *Mater. Chem. Front.*, 2025, **9**, 2844–2862.
59 X. Hu, G. Lai, Y. Liu, P. Zhou, B. Lu, Z. M. El-Bahy, M. S. Ebaid, L. Chen and J. Zhou, Design of dual-electrode interfacial kinetics regulator for long-lasting Ah-level zinc-iodine batteries, *eScience*, 2025, **5**, 100455.
60 L. Zhu, H. Zhou, D. Zhu, W. Zheng, J. Guan and K. Zhang, Achieving dendrite-free anodes for aqueous zinc ion batteries using zinc anode coated with a rGO/biomass carbon composite for interfacial modification, *Mater. Chem. Front.*, 2025, **9**, 2232–2242.
61 L. Jiang, Y. Ding, L. Li, Y. Tang, P. Zhou, B. Lu, S. Tian and J. Zhou, Cationic Adsorption-Induced Microlevelling Effect: A Pathway to Dendrite-Free Zinc Anodes, *Nano-Micro Lett.*, 2025, **17**, 202.
62 K. Zhu and W. Yang, Vanadium-Based Cathodes for Aqueous Zinc-Ion Batteries: Mechanisms, Challenges, and Strategies, *Acc. Chem. Res.*, 2024, **57**, 2887–2900.
63 Z. Li, Y. Liu, S. Yang, Z. Pan, C. Liu, X. Zhao and X. Yang, Probing Capacity Decay in Vanadium Oxide Cathodes of Aqueous Zinc-Ion Batteries Using Operando EQCM-D, *ACS Energy Lett.*, 2025, **10**, 2821–2830.
64 W. Li, W. Jiang, K. Zhu, Z. Wang, W. Xie, H. Yang, M. Ma and W. Yang, Unlocking the performance degradation of vanadium-based cathodes in aqueous zinc-ion batteries, *Chem. Eng. J.*, 2024, **496**, 153786.
65 F. Liang, M. Chen, S. Zhang, Z. Zou, C. Ge, S. Jia, S. Le, F. Yu and J. Nong, Electrochemical Activation in Vanadium Oxide with Rich Oxygen Vacancies for High-Performance Aqueous Zinc-Ion Batteries, *ACS Sustainable Chem. Eng.*, 2024, **12**, 5117–5128.
66 S. Cai, Y. Wu, H. Chen, Y. Ma, T. Fan, M. Xu and S. Bao, Why does the capacity of vanadium selenide based aqueous zinc ion batteries continue to increase during long cycles?, *J. Colloid Interface Sci.*, 2022, **615**, 30–37.
67 S. Islam, M. H. Alfaruqi, D. Y. Putro, V. Soundharrajan, B. Sambandam, J. Jo, S. Park, S. Lee, V. Mathew and J. Kim, K^+ intercalated V_2O_5 nanorods with exposed facets as advanced cathodes for high energy and high rate zinc-ion batteries, *J. Mater. Chem. A*, 2019, **7**, 20335–20347.
68 J. Wan, H. Song, J. Tian, S. Zhong and J. Liu, Recent progress and challenges of high-loading cathodes for aqueous Zn-ion batteries, *Energy Mater.*, 2025, **5**, 500090.

 This journal is © The Royal Society of Chemistry and the Chinese Chemical Society 2026